AUTOMATIC CRATER DETECTION IN 'RIDGED PLAINS' AREAS OF MARS. J. Saraiva, L.P.C. Bandeira and P. Pina, CERENA, IST, Av. Rovisco Pais, 1049-001 Lisbon, Portugal, jsaraiva@alfa.ist.utl.pt, lpcbandeira@ist.utl.pt, ppina@alfa.ist.utl.pt.

Introduction: The objective of developing a single methodology capable of dealing with the recognition of quasi-circular shapes with a wide size range in an enormous diversity of terrains is hard to achieve. Each published methodologies for automatic crater detection has its advantages and drawbacks but, so far, none has proven to be robust enough to be systematically applied and produce satisfactory results [1], [2], [3]. As a consequence, the planetary science community has shown little interest in adopting any of these approaches. Our goal, translated into a body of work that has been steadily improved through the years, is to achieve a methodology that can be applied to images of every kind of planetary surface; the various stages of its development have been chronicled in several publications [4], [5], [6]. Its general structure can be viewed in Figure 1.

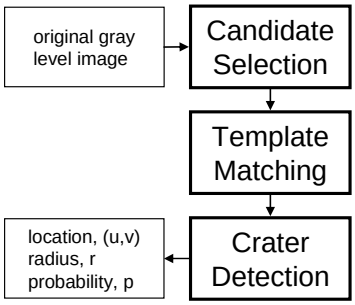

Figure 1. Fluxogram of our methodology for automated crater detection.

Dataset: We decided to apply our methodology to a large set of images neither too simplistic nor too complicated. Thus, we searched for an appropriated target, and chose the cartographic unit that was defined from Viking imagery as 'Ridged plains material' [7]. This is the basis of the Hesperian system, occupies several distinct areas on the equatorial region of Mars, and is characterized by flat plains due to volcanic flows, crossed by ridges that are older than most of the craters seen on this unit. The crater density falls midway between the heavily cratered terrains of the southern hemisphere and the almost craterless plains of the north.

The images chosen were all wide-angle MOC frames. We employed MIMS [8] to select images with a spatial resolution between 200 and 300 metres per pixel, and discarded those that were of poor quality. The final data set consisted of 101 images, pertaining to the four regions shown in Figure 2 (11, 18, 9 and 63 images in regions A, B, C and D, respectively), and covering a non-contiguous area of about 1,500,000 km^2.

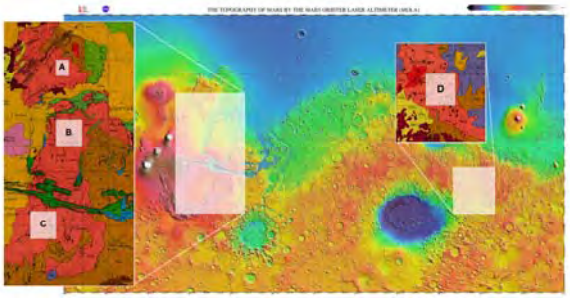

Figure 2. Location of the four areas of the Martian surface from which the images used in this paper were selected. Adapted from MOLA map and [7].

Results: To achieve a quantitative assessment of our methodology, we compare the number of impact craters that it detects on an image with the ground truth, that is, the number of craters, *GT*, that are identified visually on the same image, provided they have a diameter equal to or greater than 10 pixels.

The results presented were obtained by comparing *GT* numbers with those yielded by the automated methodology on the images contained in the data set. Two indicators were computed, the true detection rate, TDR_p, and the false detection rate, FDR_p:

$$TDR_p = \frac{TD_p}{GT} \cdot 100 \,, \; FDR_p = \frac{FD_p}{TD_p + FD_p} \cdot 100$$

where TD_p is the number of true detections and FD_p is the number of false detections, for a probability equal to or greater than p. On Table 1 the recognition rates for p=30% are presented, globally and by region.

Table 1. Crater recognition rates.

Region	*GT*	TD_{30}	TDR_{30} (%)	FD_{30}	FDR_{30} (%)
A	126	101	80.16	24	19.20
B	201	174	85.57	17	22.99
C	73	67	91.78	20	8.90
D	872	759	87.04	148	16.32
Global	1272	1101	86.57	209	15.95

The global TDR_{30}, 86.57%, and FDR_{30}, 15.95%, are very good. The best results were those of region C, but the results obtained are consistent between regions, even though the number of images and craters (*GT*) are substantially different.

In Figure 3, the automated detection of craters in image MOC E19-00650 is illustrated for two different probability levels. Fifteen impact craters respecting the conditions above were visually detected (*GT*) in this image. The figure clearly shows how the results obtained depend on the probability level that is chosen. Thus, in Figure 3a, for a probability level of 30%, there are 13 true detections (red), which means that 2 craters are missed; this represents a 86.67% success rate. There are 2 false detections (green), representing 13.33% of all the detected craters. On the right, Figure 3b, a higher probability level, 45%, leads to no false detections but also produces a reduction in true detections, now only 11, bringing the success rate down to 73.33%, still an impressive result, reinforced by the absence of false detections.

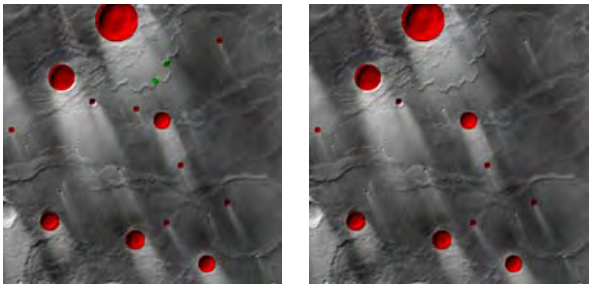

a b

Figure 3. Example of crater detection by the proposed methodology on MOC image E19-00650 [NASA/JPL/MSSS]; (a) results for p=30%; (b) results for p=45%

We computed TDR_p and FDR_p for values of p between 30 and 100% and for all images. These were plotted in Figure 4, showing how the detection rates evolve with the variation of the probability.

The higher rates are naturally obtained for the lower probability value, and correspond to the values presented in Table 1.Though both rates fall with increasing probability, FDR_p shows a sharper decrease, illustrated by the fact that for p=40% the TDR_p is still at 83.33% while the FDR_p is already a mere 5.36%. Obviously, a certain probability must be chosen in order to present a definite detection result for an image. This choice should be made according to the trade-off between TDR_p and FDR_p that is judged to best serve the final goal of any study in which this methodology can be employed (planetary mapping, chronological studies and others).

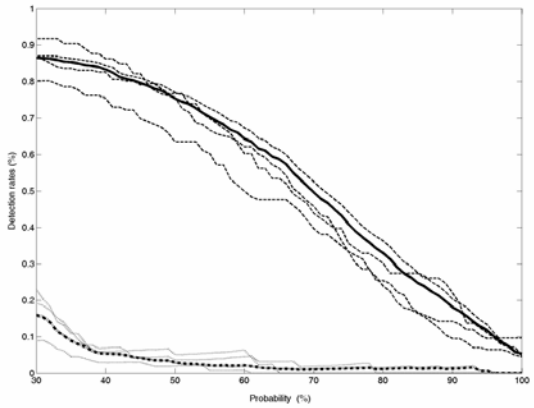

Figure 4. Variations of TDR_p and FDR_p with probability p. Global TDR_p (–), regional TDR_p (--), global FDR_p (– •) and regional FDR_p (• •).

Future Work: There are a number of intermediate steps that need to be thoroughly tested and optimized, so that they are unaffected by the characteristics of the image. The need for further testing, with images obtained by diverse sensors and with different spatial resolutions, is also recognizable. More importantly, the introduction of a verification phase, in which the marked craters will be locally assessed by a mathematical morphology operator, is planned. This should lead to the elimination of most false detections, thus allowing, in turn, for the survival of more candidates through the process of crater detection by analysis of the probability volume. In this manner, the risk of missing any true craters will be minimized. The methodology will then be able to withstand testing in larger and more geomorphologically diversified settings, from Mars and other planetary bodies of the Solar System.

References: [1] Michael G. (2003) *PSS 51*, 563-568. [2] Kim J.R. et al. (2005) *PERS 71*, 1205-1217. [3] Bue B.D. and Stepinski T.F. (2007) *IEEE Trans. Geosc. Rem. Sens. 45*, 265-274. [4] Barata T. et al. (2004) *LNCS 3212*, 489-496. [5] Saraiva J. et al. (2006) *LPS XXXVII*, Abstract #1142. [6] Bandeira L. et al. (submitted to) *IEEE Trans. Geosc. Rem. Sens.* [7] Scott D.H. and Carr M.C. (1978) Atlas of Mars. [8] Alves E.I. and Vaz D.A. (2007) *Comp. Geosc.* (in press).

Acknowledgements: This paper was developed in the frame of the project PDCTE/CTA/49724/03, funded by FCT, Portugal.